Mine Water and the Environment (2001) 20: 105–113 © IMWA Springer-Verlag 2001

Technical Article

Bulk Chemistry Analysis of Sediments from Acid Mine Lakes by Means of Wavelength Dispersive X-ray Fluorescence

Peter Morgenstern, Kurt Friese, Katrin Wendt-Potthoff, Rainer Wennrich

Centre for Environmental Research UFZ, Leipzig-Halle Ltd, Permoserstrasse 15, D-04318 Leipzig, Germany; email: morgen@ana.ufz.de

Abstract. Bulk chemistry analysis of sediments from an extremely acidic mine lake of the Lusatian lignite mining district was performed using X-ray fluorescence analysis and a wavelength dispersive spectrometer (Siemens SRS 3000). Because of pronounced changes in sample composition along the cores, we applied the fundamental parameter option for matrix correction only to the main components. The capabilities of the scattered radiation method were examined for the trace constituents.

The sediments of the acid lake were dominated by high concentrations of iron (up to 40% dry weight) in the upper horizons of depth profiles. These total iron contents were compared with values of reactive iron fractions. Aluminium and manganese concentrations were also elevated near the surface of the sediment. The concentrations of these elements decreased with depth, accompanied by changes in grain size fractions from clay to silt.

Key words: iron, mine lakes, sediment cores, scattered radiation method, X-ray fluorescence analysis

Introduction

Sediments play an important role in the biogeochemical and ecological behaviour of lakes as a source and sink for biologically relevant or toxic elements. The acid mine lake waters of the Lusatian lignite mining district are characterized by high concentrations of Fe (450 mg/l), SO_4 (2500 mg/l), Ca (340 mg/l) and several toxic elements, especially Al (45 mg/l) (Klapper and Schultze 1995; Schultze and Geller 1996; Friese et al. 1998a,b; Herzsprung et al. 1998). The sediments also reflect this chemistry (e.g.. Friese et al. 1998a; Büttner et al. 1998; Blodau et al. 1998). Mine Lake 107 (ML 107) is located in the Koyne/Plessa district about 150 km south of Berlin. It is a shallow lake (mean depth 2 m, maximum depth 5 m), approximately 70 years old, and only has groundwater inflow. The limnology of this lake is described in Lessmann et al. (1999). It is extremely acidic (pH 2.3) and wood pieces at the sediment surface show massive encrustation with iron. The special geochemical characteristics of ML 107 make it an interesting place to study the depth distributions of main and trace elements in the sediment.

In this paper, we focus on the methodical application of X-ray fluorescence (XRF) to the sediments. Because of the very strong matrix variations along the depth profiles (with 40-50% $Fe(OH)_3$ at the surface and a silicate matrix at about 20-30 cm depth), special adaptations were necessary to calibrate the analytical method under such unusual conditions. A combination of borate fusion (developed by Claisse 1957) and dilution of the extremely fine pulverized and homogenized sample material seemed to be the most suitable technique to overcome matrix effects. The fluorescence intensities measured under these conditions are free from heterogeneity and particle size effects and the calibration lines will be linear if sufficiently high dilution factors are applied. Unfortunately, this technique can be used only for the determination of major components because high dilution ratios push the concentrations below the detection limits for the trace elements.

To analyse elements in low concentrations, the scattered radiation method, first proposed by Andermann and Kemp (1958), offers a promising perspective to overcome matrix effects in undiluted samples even when large variations of matrix compositions occur within a series of specimens and suitable reference materials are not available. The application of this method to the analysis of trace elements in sediments of acid mine lakes will be a major component of this paper.

A comprehensive discussion of the theoretical background can be found in Tertian and Claisse (1982). Latest advances in application of scattered tube lines for analytical purposes were published by van Sprang and Bekkers (1998).

The use of the scattered radiation for matrix correction is especially attractive for two reasons.

First, the measured intensity of the backscattered peak already provides a relevant measure of the effective mass attenuation coefficient μ_s^* of the specimen. Second, instrumental drifts and effects due to the sample morphology can be overcome because the backscattered radiation acts as an internal standard.

Notation used:

μ_s^*	effective (combined) mass attenuation coefficient of the specimen ($\mu_{s,\lambda e} + A \cdot \mu_{s,\lambda i}$), with $A = \sin\psi_1 / \sin\psi_2$, ψ_1, ψ_2 incidence and take-off angle for primary - (λ_e) and fluorescence radiation (λ_i), respectively
$\mu_{s,\lambda I}$	mass attenuation coefficient of sample s at wavelength λ_i
C_i	concentration of analyte i
$I_{i,s}$	fluorescence intensity of analyte i
I_{scat} , I_{comp}	intensity of the scattered radiation (total and Compton portion, respectively)
σ_{scat} , σ_{comp}	mass scattering coefficient (total and Compton portion, respectively)
Q_i	proportionality constant
σ_{x0}	standard deviation of the method

Instrumentation

The measurements were carried out on a Siemens SRS 3000 X-ray fluorescence spectrometer equipped with a Rh X-ray tube (125 µm Be window), 60 kV generator, eight-position crystal changer and 58-position sample changer. The spectrometer was controlled by a PCD-3M computer with the software package SPECTRA 3000. The spectrometer operating conditions were vacuum, 34 mm collimator mask and the following analysing crystals: OVO 55, Ge, LIF 100 and LIF 110. The Rh K_α Compton scattered tube line, used for analytical purposes, was recorded with the 0,15° collimator in combination with the LIF 110 crystal and the NaI scintillation counter (Figure 1). Two background positions were chosen to calculate net count rates.

Sampling

Sediments from ML107 were sampled during May 1997. Undisturbed sediment cores were collected using a modified Kajak gravity corer (Uwitec, Mondsee, Austria). Depending on the sample site, the top 15 to 40 cm of sediment and 10 to 30 cm of overlying water were recovered in polycarbonate tubes (50 cm in length, 9 cm ID). Sediment subsamples were extruded and sectioned in 1 cm vertical intervals in the field immediately after sampling. The samples were transferred into polypropylene screw cap vials, which were completely filled to minimize oxygen contact. Samples were kept on ice and transported to the laboratory within 3 days.

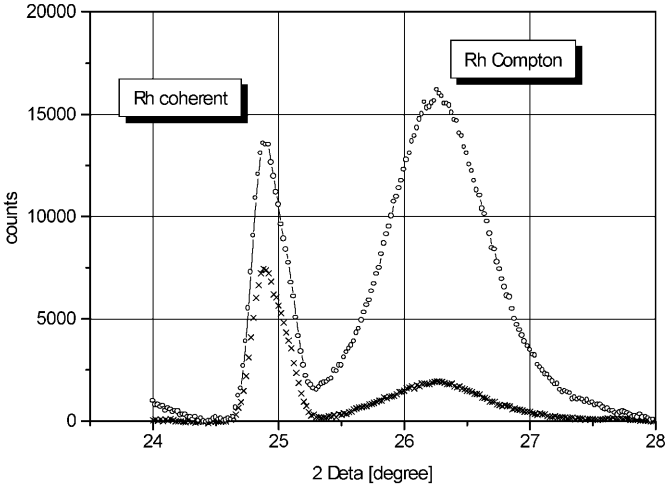

Figure 1. Rh K_α coherent - and Compton scattered radiation for SiO_2 (ooo) and Fe_2O_3 (×××) matrix.

Sample preparation

The reactive iron (HCl-soluble and hydroxylamine-reducible) fractions were determined from the fresh sediment material using ferrozine according to Lovley & Phillips (1987). The hydroxylamine fraction yields both Fe(II) and poorly crystalline Fe(III) phases. Briefly, triplicate subsamples were extracted in either 0.5 M HCl or 0.25 M hydroxylamine hydrochloride in 0.25 M HCl for 1 h on a test tube rotator. Aliquots were transferred to ferrozine solution in 50 mM HEPES buffer, and centrifugation was used instead of filtration to retrieve clear solutions for photometric analysis. This method generally yielded relative standard deviations of 5% for HCl and 7% for hydroxylamine extraction (Friese et al. 1998b).

For the XRF studies, the sample material was dried at 105°C and ground by means of an agate ball mill (Retsch) to meet the conditions of homogenized and analytical grade material. Aliquots (4 g) of the prepared sample material were mixed with 20 % wax (Hoechst wax for XRF-analysis) as a binder, poured into dies and compacted in a hydraulic press at a pressure of 100 MPa. Other parts of the sample

powder were diluted with $Li_2B_4O_7$ (1 g sample + 7 g $Li_2B_4O_7$) to prepare glass discs by fusion at 1200°C in a 95% platinium-5% gold crucible for 20 min. Each batch was checked for loss on ignition (LOI).

To examine both the theoretically predicted and the experimentally observed dependence of the scattered radiation on the mass attenuation coefficient of the sample matrix, a set of pressed samples was prepared to cover a wide range of matrix compositions similar to that occuring along the sediment profiles of the investigated acid mine lake. These artifical standards were produced by successive addition of Fe_2O_3 to SiO_2 powder. In addition to this, a carbon matrix specimen from the reference material BCR 40(certified coal) was included. The effective mass attenuation coefficient of this set of standards varied by more than one order of magnitude for the Rh-K_α tube line.

Theoretical background of the scattered radiation method

Without enhancement by the matrix, the fluorescence intensity of element i at concentration C_i in a specimen s is given by:

$$I_{i,s} = \frac{Q_i \cdot C_i}{\mu_s^*} \qquad (1)$$

(Tertian and Claisse 1982). According to Hower's rule (1959), $\mu_{s,\lambda 1}/\mu_{s,\lambda 2}$ is a constant if no major elements including the analyte have an absorption edge between the two radiations, so equation (1) can be written as

$$I_{i,s} \sim \frac{C_i}{\mu_{s,\lambda i}} \qquad (2)$$

In the same way, the scattered intensity of a given irradiation line can be calculated:

$$I_{scat} \sim \frac{\sigma_{scat}}{\mu_{s,\lambda i}} \qquad (3)$$

Because both the intensity of the scattered radiation(3) and the intensity of a fluorescence line (2), are proportional to $1/\mu_{s,\lambda i}$, the ratio $I_{i,s}/I_{scat}$ becomes independent of $\mu_{s\lambda i}$ and is therefore directly proportional to concentration C_i of the analyte i.

However, the considerations made above are valid only if the mass scattering coefficient σ_{scat} does not significantly vary with the atomic number Z of the scattering target. Theoretical calculations (Tertian and Claisse 1982) show that only the Compton scattered radiation fulfills this condition approximately, decreasing only slowly with increasing Z while the coherent scattering coefficient increases rapidly with Z. That means, equation (3) is approximately valid only for the Compton part of the scattered tube line

$$I_{comp} \sim \frac{\sigma_{comp}}{\mu_{s,\lambda Rh}} \qquad (4)$$

To take into account the slow dependence $\sigma_{comp} = \sigma_{comp}(Z)$, it seems to be useful to express σ_{comp} as a function of the mass attenuation coefficient of the sample. Although there exists no theoretical background for a dependence $\sigma_{comp} = \sigma_{comp}(\mu_s)$, many publications deal with different empirical approaches in connection with the solution of specific analytical problems. A promising approach $\sigma_{comp} = \sigma_{comp}(\mu_s)$ was initiated by Sheng Xiang Bao (1997), who used a power function for $\sigma_{comp}(\mu_s)$, which successfully reproduced the experimental results over a wide range of compositions.

Experimental studies of the scattered radiation method

Comparison of theoretical and experimental results

For the set of artifical standards described above, the Compton part of the mass scattering coefficient σ_{comp} was calculated on the base of the tabulated values of the non relativistic Hartree-Fock wave functions published by Hubbell et al. (1975) (for Rh K_α and a scattering angle of 90°) and related to the calculated mass attenuation coefficients of the corresponding sample compositions (Figure 2). A linear correlation plot of the values log ($\mu_{s,Rh\text{-}K}$) as a function of log $(\sigma_{comp}/\mu_{s,Rh-K})^{-1}$ of the calculated values for $\mu_{s,\lambda Rh}$ and σ_{comp} leads to the expression

$$(\sigma_{comp})_{theor} = 0{,}0101 \cdot \mu_{s,\lambda Rh}^{-0{,}046} \qquad (5)$$

Otherwise, a logarithmic relationship between the mass attenuation coefficient $\mu_{s,\lambda Rh}$ of the investigated samples and the measured inverse Compton peak intensity of the scattered $Rh_{K\alpha}$ tube line (see Figure 3) yields:

$$\mu_{s,\lambda Rh} \sim \frac{1}{I_{comp}^{0{,}947}} \qquad (6)$$

With respect to equation 4, the experimentally found relation (6) gives

$$(\sigma_{comp})_{exp} \sim \mu_{s,\lambda Rh}^{-0{,}055} \qquad (7)$$

In Figure 2, it is demonstrated that the theoretically estimated dependence of the mass scattering coefficient on the mass attenuation coefficient $\mu_{s,\lambda Rh}$ (5) can be successfully fitted almost over the whole range of the investigated matrix compositions by the empirically found approch (7). Inaccuracies for σ_{comp} >0,01 cm^2 / g·sr are probably due to higher order effects (see also van Sprang and Bekkers 1998). With respect to equation (2) and (6), we finally find

$$\frac{I_{i,s}}{I_{comp}^{0,947}} \sim C_i \qquad (8)$$

That means the ratio ($I_{i,s} / I_{comp}^{0,947}$) becomes a matrix independent value and is directly proportional to the concentration C_i of analyte i over the whole range of the investigated matrix compositions.

Efficiency of the empirically found approch

To control the efficiency of the experimentally found correction algorithm, typical sediment material originating from the surface of the sediment profile K 18 from ML 107 was diluted with the reference material GBW 07310 (stream sediment), in which the investigated trace elements occur at nearly the same concentration levels as in the investigated lake sediment. This was verified by analysis of aqua regia extracts of sediment samples using ICP-OES and graphite furnace atomic absorption spectrometry (GF-AAS). In this way, a set of samples was created in which the investigated trace elements were hold at a nearly constant concentration level, while simultaneously the sample matrix significantly changed from $Fe(OH)_3$ to SiO_2 (see table 1).

To check the accuracy of the investigated correction algorithm, the concentration values determined in the original sediment sample were compared with the corresponding data measured in the diluted specimens, using relation (9).

$$C_{i,Sed} = \frac{C_{i,Sed,D} - C_{i,ref} \cdot (1 - D)}{D} \qquad (9)$$

where $C_{i,Sed}$= concentration of analyte i in the original sediment

$C_{i,Sed,D}$ = measured concentration of analyte i in the diluted sample

$C_{i,ref}$ = concentration of analyte i in the reference material and

D= dilution factor $[mass_{Sed}/(mass_{ref} + mass_{Sed})]$.

In Tables 1 and 2, the experimental results of these measurements are displayed. The uncertainties of the results of the scattered radiation method were derived from the validation data given in table 3 (at a significance level of 95%). If we take into account these uncertainties, no sytematic deviations can be observed comparing the data derived from the diluted specimens with the concentration values determined in the undiluted sample, although the mass attenuation coefficient $\mu_{s,Rh}$ of the specimen changed from 2,4 to about 6,7 cm^2/g.

In Table 2, additional results for the analytes under study are listed, based on ICP-OES and GF-AAS determinations. These measurements are only for information and were performed to provide a measure for the concentration levels of trace elements by means of a reference method and to enable us to select a suitable reference material, which can act as diluent. Before comparing the ICP-OES and GF-AAS results with the XRF data, one should consider that due to the differences in sample preparation, XRF data represent the total content of elements in the solid material, while the ICP-OES and GF-AAS measurements are based on a leaching procedure (aqua regia). In addition, there are also several uncertainties in the determination of the trace elements Cu, As and Pb using ICP-OES because of interferences by the matrix of the investigated sediment, which contains high amounts of iron.

Calibration and measurements

Major elements

Glass discs were prepared by fusion of reference materials (coal fly ashes: NBS 2689 and NBS 2691, lake and stream sediments: LKSD 1-4; STSD 1-4) to calibrate the analytes Na_2O, MgO, Al_2O_3, SiO_2, P_2O_5, K_2O, CaO, Ti_2O, MnO and Fe_2O_3. For sulphur calibration, pressed powder samples were prepared including the geochemical reference materials BAF, BE-1, and BAF BS-1.

The measured fluorescence intensities of each analyte were corrected by means of the fundamental parameter algorithm, to get linear calibration plots for all main constituents. This procedure is state of the art and was provided by the spectrometer software SPECTRA 3000. The concentrations of the unknowns derived from these calibration plots were automatically related to the undiluted material by the software.

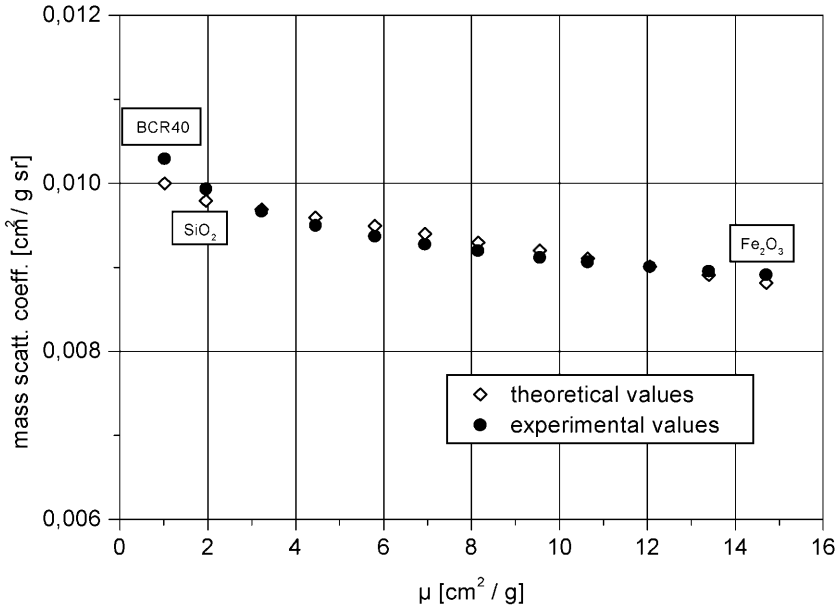

Figure 2. Dependence of the mass scattering coefficient σ_{comp} [$cm^2/g \cdot sr$] (for the Rh K_α tube line) on the mass attenuation coefficient $\mu_{s,\lambda Rh}$ of the sample matrix for a set of standards described above. ◊◊◊ data based on the theoretically estimated values of σ_{comp}. ••• data based on the empirically derived approch $\mu_{s,\lambda Rh} \sim \frac{1}{I_{comp}^{0,947}}$.

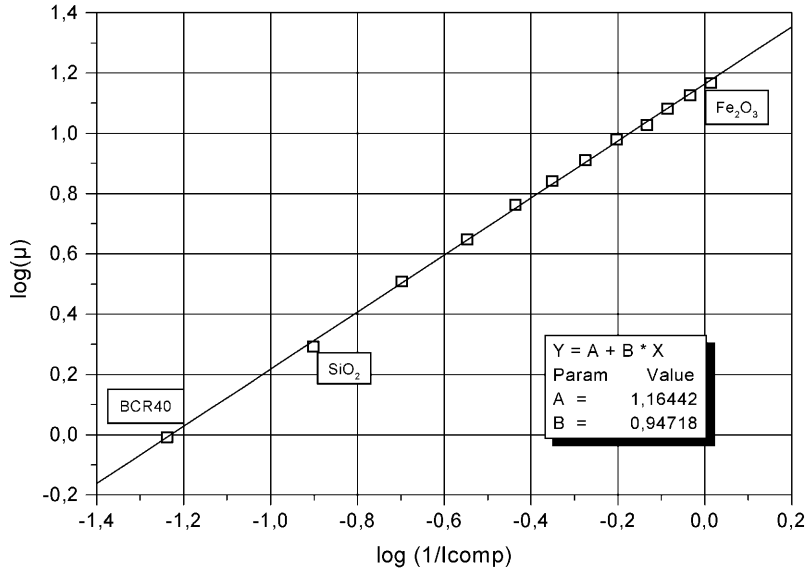

Figure 3. Logarithmic relationship between mass attenuation coefficient and inverse Compton peak intensity of the Rh K_α line for the set of artifical standards.

Table 1. Analytical results for the trace elements Ni, Cu, Zn, As and Pb, analyzing a sediment sample of ML107 by matrix dilution with the reference material GBW07310 ($C_{i,Sed,Dj}$ is the measured concentration obtained for the dilution D_j)

$mass_{Sed}$	$mass_{ref}$	D_j	$C_{Ni,Sed,Dj}$	$C_{Cu,Sed,Dj}$	$C_{Zn,Sed,Dj}$	$C_{As,Sed,Dj}$	$C_{Pb,Sed,Dj}$
g	g		mg/kg	mg/kg	mg/kg	mg/kg	mg/kg
4,0	0,0	1,0	9	32	38	16	29
3,6	0,4	0,9	14	28	39	17	26
3,2	0,8	0,8	15	30	40	16	28
2,4	1,6	0,6	18	28	40	18	28
1,6	2,4	0,4	23	26	42	21	26
0,0	4,0	0,0	28	21	45	22	26
GBW07310		certified	30	23	46	25	27

Table 2. Comparison of the analytical results, obtained for the undiluted sediment with the concentration values calculated from the results determined in the diluted specimens (see table 1). (ICP-OES/GF-AAS data for information only).

sample	method		Ni	Cu	Zn	As	Pb
			mg/kg	mg/kg	mg/kg	mg/kg	mg/kg
Sediment	scattered radiation	undiluted*	9 +/- 4	32 +/-3	38 +/-3	16 +/-3	29 +/-3
ML 107	method	diluted**	11	31	37	15	27
	ICP-OES/GF-AAS	aqua regia	6	16	39	16	21

undiluted* - data determined in the undiluted specimen; diluted** - mean of the results calculated from the data obtained for the diluted specimens (table 1)after correction by equation (9).

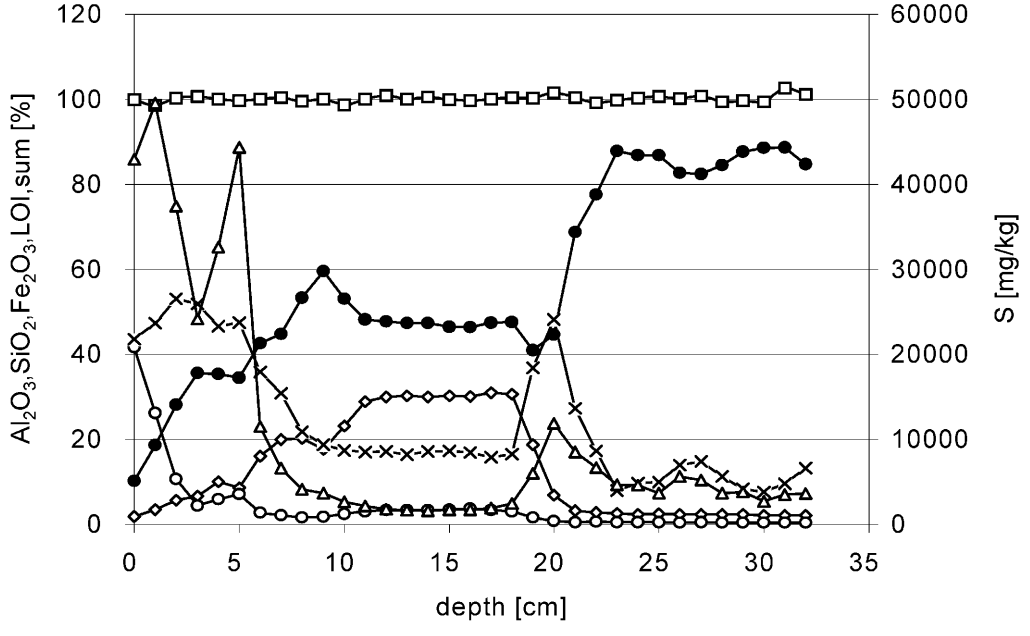

Figure 4. Al_2O_3 (◊◊◊), SiO_2(•••), S(ΔΔΔ), Fe_2O_3(ooo) concentrations, LOI(×××) values and the sum(□□)of all, along the sediment core K18 from ML 107.

In Figure 4, the analytical results of the sediment core K18 from ML 107 are displayed as an example, demonstrating the typical depth distribution of the matrix composition of the investigated sediment cores. The corresponding LOI values, which were estimated by weighting the sample before and after fusion, are

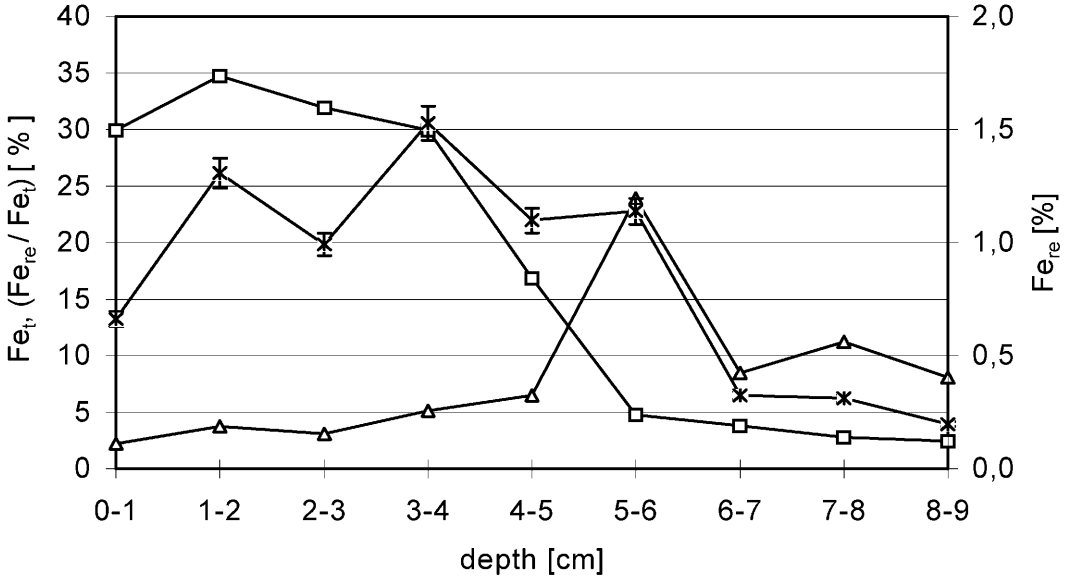

Figure 5. Fe content (% of dry weight) in a sediment core from ML 107. Fe total (Fe_t □□) as determined by WDXRF, reactive Fe (Fe_{re} ×××) as determined by hydroxylamine extraction and the contribution of highly reactive Fe to the total Fe pool (Fe_{re}/Fe_t ΔΔΔ).

represented too. The measured data illustrate the strong matrix variations along the sediment profile. Near the surface, Fe dominated the sediment matrix but decreased dramatically with depth. The increase of Al and Si in the upper 12 cm point to an increasing contribution of clay minerals. Below 19 cm depth, Si became the dominant element and LOI decreased sharply. This is indicative of pure tertiary sand and therefore marks the end of the authigenic lake sediment.

To provide a control for the accuracy of the measured data, the sum of all concentrations measured by means of wavelength dispersive X-ray fluorescence (WDXRF) and the LOI values are also presented in Figure 4. The sum of the major components equals 100%, showing that accurate measurements were achieved. The total iron concentrations measured by WDXRF were further used as a basis to determine the fraction of highly reactive iron in the sediment of ML 107 (Figure 5). Only a minor part of the total iron was extractable by the hydroxylamine method. This implies that the iron in the upper centimetres of this core does not contain significant amounts of freshly precipitated amorphous hydroxides. So most of the iron in ML 107 sediment is probably not microbially available, although hydroxylamine might not extract this fraction completely (Lovley & Phillips, 1986, 1987). However, the increased fraction of reactive Fe at 5-6 cm was due to HCl-soluble Fe(II) (data not shown), indicating that Fe(III) reduction occured in ML107.

Trace Constituents

For determination of the trace constituents, calibration plots based on expression (8) were created. The required parameters for a linear relationship between the ratio ($I_{i,s}/I_{comp}^{0,947}$) of an analyte and the concentration were adjusted by measuring a set of reference materials (stream sediment:GBW 07309 - GBW 07312 and soils: GBW 07402, GBW 07406 -07, GBW 07409 - GBW07411) prepared as infinite thick pellets. The experimental data were fitted by a regression routine. In Table 3, the standard deviations of the method for the elements Ni, Cu, Zn, As and Pb are given. The displayed data were derived from the corresponding calibration curves using the validation software package SQS 98 (Perkin Elmer).

As an example, experimental results applying the scattered radiation method to investigate the depth distribution of the trace constituents Ni, Cu, Zn, As and Pb in the sediment core K18 from ML 107 are displayed in Figure 6.

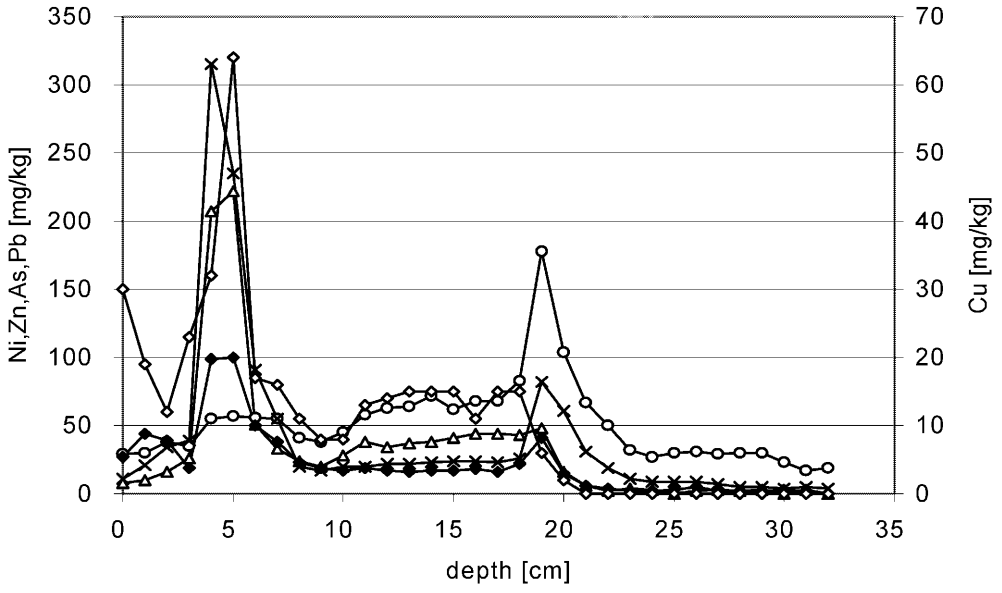

Figure 6. Depth distribution of the trace constituents Ni (ΔΔΔ), Cu(◊◊◊), Zn(ooo), As(×××) and Pb(♦♦♦) for the sediment core K18 from ML 107

Table 3. Standard deviation of the method for the calibration plots of Ni, Cu, Zn, As and Pb in the concentration range 2-500 mg/kg, applying the empirically found approach $C_i \sim \frac{I_{i,s}}{I_{comp}^{0,947}}$.

Analyte	σ_{x0} [mg/kg]
Ni	3
Cu	2
Zn	2
As	3
Pb	2

Conclusions

The results of the methodological application of WDXRF to the unusual composition of sediments from an acid mine lake lead to an accurate and rapid method for determination of main and trace elements in such kind of samples. It could be shown that the experimen tally found scattered radiation algorithm successfully corrects the strong matrix effects along the depth profiles of the investigated sediment cores.

Total contents of biogeochemically relevant elements determined by WDXRF will provide a valuable basis for comparison and control when selected fractions are measured by operationally defined extraction methods.

Acknowledgements

The authors gratefully acknowledge the assistance of T Bachmann, M Herzog, S Kellner, B Lohrmann, G Packroff, B Scharf and C Scholz during field work. This work was financially supported in part by the German Ministry for Education, Science, Research and Technology (BMBF, Fkz. 0339684 and Fkz. WB2 9596/6).

References

Andermann G, Kemp JW (1958) Anal. Chem. 30, 1306 (cited in Tertian and Claisse 1982, Principles of Quantitative X-Ray Fluorescence Analysis, Heyden, London)

Blodau C, Hoffmann S, Peine A, Peiffer S (1998) Iron and sulfate reduction in the sediments of acidic mine lake 116 (Brandenburg, Germany): Rates and geochemical evaluation. Water, Air and Soil Pollution 108: 249-270

Büttner O, Becker A, Kellner S, Kuehn B, Wendt-Potthoff K, Zachmann DW, Friese K (1998) Geostatistical analyses of surface sediments in an acidic mining lake. Water, Air and Soil Pollution 108: 297-316

Claisse F, Norelco Rep 4(3), 95 (1957) (cited in Tertian and Claisse 1982, Principles of Quantitative X-Ray Fluorescence Analysis, Heyden, London)

Friese K, Hupfer M, Schultze M (1998a) Chemical characterization of water and sediment in acid mining lakes of the Lusatian lignite district, In: Geller W, Klapper H, Salomons W (Eds), Acidic Mining Lakes - Acid Mine Drainage, Limnology and Reclamation, Springer, Berlin, pp 25-45

Friese K, Wendt-Potthoff K, Zachmann DW, Fauville A, Mayer B, Veizer J (1998b) Biogeochemistry of iron and sulfur in sediments of an acidic mining lake in Lusatia, Germany. Water, Air and Soil Pollution, 108: 231-247

Herzsprung P, Packroff G, Schimmele M, Wendt-Potthoff K, Winkler M, Friese K (1998) Vertical and annual distribution of ferric and ferrous iron in acidic mining lakes. Acta hydrochim hydrobiol, 26: 253-262

Hower J (1959) Am. Mineral., 44:19. (cited in Tertian and Claisse 1982, Principles of Quantitative X-Ray Fluorescence Analysis, Heyden, London)

Hubbell JH, Veigele WJ, Briggs EA, Brown RT, Cramer DT, Howerton RJ (1975) Atomic Form Factors, Incoherent Scattering Functions, and Photon Scattering Cross Sections, J Phys Chem Ref Data 4, 471

Klapper H, Schultze M (1995) Geogenically acidified mining lakes - living conditions and possibilities of restoration. Int. Revue ges. Hydrobiol. 80: 639-653

Lessmann D, Deneke R, Ender R, Hemm M, Kapfer M, Krumbeck H, Wollmann K, Nixdorf B (1999) Lake Plessa 107 (Lusatia, Germany) - an extremely acidic shallow mining lake. Hydrobiologia, 408/409: 293-299

Lovley DR, Phillips EJP (1986) Availability of ferric iron for microbial reduction in bottom sediments of the freshwater tidal Potomac River, Appl. Environ. Microbiol. 52: 751-757

Lovley DR, Phillips EJP (1987) Rapid assay for microbially reducible ferric iron in aquatic sediments. Appl Environ Microbiol 53:1536-1540

Schultze M, Geller W (1996) The acid lakes of lignite mining district of the former German Democratic Republic, In: Reuther R (Ed), Geochemical approaches to environmental engineering of metals, Environ. Sci. Series, Springer, Heidelberg, pp 89-105

Sheng XB (1997) A power function relation between mass attenuation coefficient and Rh K_α Compton peak intensity and its application to XRF analysis, X-Ray Spectrom. 26: 23-27

Tertian R, Claisse F (1982) Principles of Quantitative X-Ray Fluorescence Analysis, Heyden, London

van Sprang HA, Bekkers MHJ (1998) Analytical implications of using scattered tube lines, X-Ray Spectrom. 27 31-36